

# EFFICIENT COMPUTATION OF OPTIMAL LOW THRUST GRAVITY PERTURBED ORBIT TRANSFERS

Robyn Woollands<sup>\*†</sup>, Ehsan Taheri<sup>‡</sup>, and John L. Junkins<sup>§</sup>

We have developed a new method for solving low-thrust fuel-optimal orbit transfer problems in the vicinity of a large body (planet or asteroid), considering a high-fidelity spherical harmonic gravity model. The algorithm is formulated via the indirect optimization method, leading to a two-point boundary value problem (TP-BVP). We make use of a hyperbolic tangent smoothing law for performing continuation on the thrust magnitude to reduce the sharpness of the control switches in early iterations and thus promote convergence. The TPBVP is solved using the method of particular solutions (MPS) shooting method and Picard-Chebyshev numerical integration. Application of Picard-Chebyshev integration affords an avenue for increased efficiency that is not available with step-by-step integrators. We demonstrate that computing the particular solutions with only a low-fidelity force model greatly increases the efficiency of the algorithm while ultimately achieving near machine precision accuracy. A salient feature of the MPS is that it is parallelizable, and thus further speedups are available. It is also shown that, for near-Earth orbits and over a small number of en-route revolutions around the Earth, only the zonal perturbation terms are required in the costate equations to obtain a solution that is accurate to machine precision and optimal to engineering precision. The proposed framework can be used for trajectory design around small asteroids and also for orbit debris rendezvous and removal tasks.

## INTRODUCTION

Designing optimal spacecraft orbit maneuvers using both continuous and impulsive thrust has been the subject of interest for several decades.<sup>1-5</sup> The challenge of accurately and efficiently finding fuel- or time-optimal solutions for an orbit transfer where many variables, constraints and numerical limitations are present is still an active area of research.<sup>6-8</sup> Many approaches have been proposed for solving these problems, and they typically fall into one of two categories: direct methods or indirect methods.<sup>9</sup> Sometimes hybrid methods are used, which combine the two techniques. A review of models, objectives, approaches and solutions is presented in.<sup>10</sup>

Direct methods involve formulating the optimization problem as a nonlinear programming (NLP) problem whereby the states and controls are parameterized using a set of basis functions and the parameters are iteratively updated until a solution is obtained. A drawback of these methods is that they do not make use of Pontryagin's maximum principle (PMP)<sup>11</sup> to ensure at least local optimality,

\*Aerospace GNC Engineer, Jet Propulsion Laboratory, California Institute of Technology, Pasadena, CA 91109

†Adjunct Assistant Professor, Department of Aerospace Engineering, Texas A&M University, College Station, TX 77843-3141, Member AAS.

‡Research Assistant Professor, Department of Aerospace Engineering, Texas A&M University, College Station, TX 77843-3141, Member AAS.

§Distinguished Professor, Department of Aerospace Engineering, Texas A&M University, College Station, TX 77843-3141, Fellow AAS.

and in general many parameters are required to obtain an accurate sub-optimal solution using either collocation or a shooting method.<sup>12,13</sup> On the other hand, a positive attribute of these methods is that they typically have lower sensitivity with respect to starting estimates, and it is frequently possible to adaptively increase the dimensionality with the highest required dimensionality used only for final iterations. Significant historical contributions to direct methods have been made by Hargraves and Paris,<sup>12</sup> Betts,<sup>14</sup> Enright and Conway,<sup>15,16</sup> Seywald<sup>17</sup> and others.

Indirect methods seek to satisfy PMP by applying the necessary conditions for optimality. Although these methods ensure that the solution is at least a local extremum, they result in boundary-value problems that are usually very sensitive to an initial starting iterative and convergence is not guaranteed. Indirect methods are frequently solved approximately with collocation where the state equations, costate equations and prescribed boundary conditions are satisfied approximately through parameterization using basis functions. The dimension of the unknown parameter vector grows as higher accuracy is sought. However, even with limitation, practical results can be obtained for many problems and the resulting sub-optimal solution can be used to start a corresponding indirect algorithm. With a good initial guess for the costates, a shooting method may be utilized to solve the Pontryagin necessary conditions and thus converge to a solution that meets the prescribed final boundary conditions. Significant contributions to indirect methods have been made by Bryson,<sup>11</sup> Miele,<sup>18-21</sup> Brusch,<sup>22</sup> Hull,<sup>23</sup> and Conway.<sup>24</sup>

In this paper, we present a method for solving the optimal low-thrust fuel-optimal orbit transfer problems in the vicinity of a large body (planet or asteroid) where a high-fidelity spherical harmonic gravity model is required. The algorithm is formulated via the indirect variational calculus approach which leads to a two-point boundary-value problem (TPBVP). The choice of coordinates for formulating and solving a problem is important as it can effect the numerical convergence properties of the solution method.<sup>25,26</sup> Therefore, we select the regularized modified equinoctial elements (MEEs) because five out of the six elements vary slowly with time and generally result in increases in the domain of convergence when solving TPBVPs via a shooting method.

We make use of a hyperbolic tangent smoothing law for performing continuation on the thrust magnitude to reduce the sharpness of the control switches in early iterations and thus promote convergence.<sup>27,28</sup> The TPBVP is solved using a single-shooting scheme that utilizes the method of particular solutions (MPS)<sup>29</sup> and Picard-Chebyshev numerical integration. Any integrator can be used for propagating the resulting set of state/costate dynamics with MPS, however, we show that using Picard-Chebyshev integration affords an avenue for increased efficiency that is not available with other step-by-step integrators. We demonstrate that computing the particular solutions with only a low-fidelity force model greatly increases the efficiency of the algorithm while ultimately achieving near machine precision accuracy. We also show that for Earth-bound orbits only the zonal harmonic terms are required in the costate equations to obtain a solution that is accurate to near machine precision and therefore, optimal to engineering precision.

One application for this work is to respond to the various challenges in Space Situational Awareness (SSA). The recent satellite collisions of Iridium and Cosmos in 2009,<sup>30</sup> and the intentional destruction of China's Fengyun satellite in 2007,<sup>31</sup> greatly increased the number of orbiting objects and elevated the already challenging SSA problem. As of 2013 we could track over 20,000 fragmented debris objects, over 1,500 mission-related debris, and over 1,500 rocket bodies orbiting the Earth.<sup>32</sup> This number will increase by an order of magnitude with the advent of the new radar space fence by 2020. Optimal control (e.g., fuel-optimal) trajectories can be utilized to compute extremal orbit transfers to see if spacecraft A can reach spacecraft B in a prescribed time window.

Orbital debris is hazardous to operational satellites and reducing the risk of collisions is possible by orbit debris rendezvous, capture and de-orbit missions directed at the most high priority debris objects. The cost of launching a spacecraft with large conventional propulsion systems to make plane changes to capture debris makes conventional propulsion approaches to debris removal extremely expensive. Therefore low thrust propulsion technology is attractive because much lower mass debris capture spacecraft are feasible. Advancing the state of the practice for accurate and efficient optimization of low-thrust maneuvers, using methods such as Picard-Chebyshev iteration and MPS, that to date have not been used to tackle the optimal perturbed orbit transfer problem, are promising avenues worth pursuing.

## INDIRECT OPTIMAL CONTROL FORMULATION

We consider the problem of a spacecraft orbiting a large irregular body such as a planet or an asteroid where a high-fidelity gravity model is included in the dynamics. We adopt the MEEs as state variables and include the variation of mass due to propellant spent as a function of time. MEEs are well-suited to the optimization of low-thrust trajectories as they allow the most general representation that includes circular, elliptic and hyperbolic orbits without singularities at zero eccentricities and inclinations. In addition, five of the six MEEs are considered “slow variables” as they vary slowly with time. The sixth variable, the true longitude ( $l$ ) is a fast variable and is a near linear function of time. In contrast, the six Cartesian coordinates are all “fast variables” as they have more nonlinear dynamics. Slow variables are particularly attractive from a numerical method standpoint as slow variables remain in the linear domain for longer and thus increase the domain over which TPBVP solvers will converge (i.e. shooting methods). In a set of recent papers, Taheri et al.<sup>25</sup> and Junkins and Taheri<sup>26</sup> demonstrated the superiority of regularized element sets (including the MEEs) over traditional Cartesian and spherical coordinate when they are used to formulate optimal orbit transfer problem.

### Equations of Motion

The MEEs ( $p, f, g, h, k, l$ ) are related to the classical orbit elements ( $a, e, i, \Omega, w, \nu$ ) through the following set of equations:

$$\begin{aligned} p &= a(1 - e^2), & f &= e \cos(\Omega + w), & g &= e \sin(\Omega + w), \\ h &= \tan\left(\frac{i}{2}\right) \cos(\Omega), & k &= \tan\left(\frac{i}{2}\right) \sin(\Omega), & l &= \Omega + w + \nu, \end{aligned}$$

where  $a$  is the semimajor axis,  $e$  is the eccentricity,  $i$  is the inclination,  $\Omega$  is the right ascension of the ascending node,  $w$  is the argument of perigee and  $\nu$  is the true anomaly.

Let  $\mathbf{x} = [p, f, g, h, k, l]^\top$  denote the vector of MEEs and let  $\mathbf{a}_d = [a_r, a_t, a_n]^\top$  and  $\mathbf{u}_T = [u_r, u_t, u_n]^\top$  denote the vector of perturbing gravitational accelerations and the vector of thrust acceleration respectively, with components in the local-vertical/local-horizontal (LVLH) reference frame. Let  $\mathbf{u} = \mathbf{a}_d + \mathbf{u}_T$  denote the total acceleration expressed in the LVLH frame, the dynamics of MEEs can be written as

$$\dot{\mathbf{x}} = \mathbf{A}(\mathbf{x}) + \mathbb{B}(\mathbf{x})\mathbf{u}, \quad (1)$$

where  $\mathbf{A}(\mathbf{x})$  denotes the unforced part of the dynamics

$$\mathbf{A}(\mathbf{x}) = \begin{bmatrix} 0 & 0 & 0 & 0 & 0 & \sqrt{\mu p} \left(\frac{w}{p}\right)^2 \end{bmatrix}^\top, \quad (2)$$

and  $\mathbb{B}(\mathbf{x})$  denotes the control influence matrix

$$\mathbb{B}(\mathbf{x}) = \begin{bmatrix} 0 & \frac{2p}{w} \sqrt{\frac{p}{\mu}} & 0 \\ \sqrt{\frac{p}{\mu}} \sin(l) & \sqrt{\frac{p}{\mu}} \frac{1}{w} [(w+1) \cos(l) + f] & -\sqrt{\frac{p}{\mu}} \frac{g}{w} [h \sin(l) - k \cos(l)] \\ -\sqrt{\frac{p}{\mu}} \cos(l) & \sqrt{\frac{p}{\mu}} \frac{1}{w} [(w+1) \sin(l) + g] & \sqrt{\frac{p}{\mu}} \frac{f}{w} [h \sin(l) - k \cos(l)] \\ 0 & 0 & \sqrt{\frac{p}{\mu}} \frac{s^2 \cos(l)}{2w} \\ 0 & 0 & \sqrt{\frac{p}{\mu}} \frac{s^2 \sin(l)}{2w} \\ 0 & 0 & \sqrt{\frac{p}{\mu}} \frac{1}{w} [h \sin(l) - k \cos(l)] \end{bmatrix}. \quad (3)$$

The dynamical model including the variation of the mass, the control and the gravitational perturbations are written as

$$\dot{\mathbf{x}} = \mathbf{A}(\mathbf{x}) + \mathbb{B}\mathbf{a}_d + \frac{T}{m} \mathbb{B}\hat{\mathbf{P}}\delta, \quad (4)$$

$$\dot{m} = -\frac{T}{c} \delta, \quad (5)$$

where the thrust direction  $\mathbf{u}_T = \hat{\mathbf{P}}\delta$ . In the above equations  $m$  is the mass of the spacecraft,  $T$  is the maximum allowable thrust,  $0 \leq \delta \leq 1$  is the engine throttle, and  $c = I_{sp}g_0$  is the exhaust velocity.  $I_{sp}$  and  $g_0$  are the specific impulse and the gravitational acceleration at sea level and  $\hat{\mathbf{P}}$  denotes the thrust steering unit direction vector. It is assumed that the spacecraft uses a constant specific impulse (CSI) engine in which the maximum achievable thrust level and the specific impulse value are both constant for all test cases.

### Minimum-Fuel Bang-Bang Control

For minimum-fuel problems, the cost functional to be minimized can be written in terms of the propellant mass  $m_p$  consumed as

$$J = \frac{T}{c} \int_{t_0}^{t_f} \delta dt. \quad (6)$$

The control inputs being optimized are  $\mathbf{\Gamma}$  and  $\delta$ . The Hamiltonian is formulated as follows

$$H = \frac{T}{c} \delta + \boldsymbol{\lambda}^\top \left[ \mathbf{A} + \mathbb{B}\mathbf{a}_d + \frac{T}{m} \mathbb{B}\hat{\mathbf{P}}\delta \right] - \lambda_m \frac{T}{c} \delta, \quad (7)$$

where  $\boldsymbol{\lambda} = [\lambda_p, \lambda_f, \lambda_g, \lambda_h, \lambda_k, \lambda_l]^\top$  is the costate vector associated with the MEEs and  $\lambda_m$  is the costate associated with the mass. Their dynamics is obtained by the Euler-Lagrange relation

$$\dot{\boldsymbol{\lambda}} = - \left[ \frac{\partial H}{\partial \mathbf{x}} \right]^\top, \quad (8)$$

$$\dot{\lambda}_m = - \frac{\partial H}{\partial m}. \quad (9)$$

Expanding and rearranging the terms in the Hamiltonian leads to

$$H = \frac{T}{c} \delta + \boldsymbol{\lambda}^\top \mathbf{A} + \boldsymbol{\lambda}^\top \mathbb{B}\mathbf{a}_d + \frac{T}{m} \boldsymbol{\lambda}^\top \mathbb{B}\hat{\mathbf{P}}\delta - \lambda_m \frac{T}{c} \delta. \quad (10)$$

The Hamiltonian is a linear function of both the unit thrust direction vector  $\hat{\mathbf{P}}$  and the throttling magnitude  $\delta$ . Therefore, from PMP we can characterize the optimal (superscript ‘\*’) thrust vector,

$$\hat{\mathbf{P}}^* = \arg \min_{\|\hat{\mathbf{P}}\|=1} H. \quad (11)$$

The Hamiltonian is minimized, following Lawden,<sup>33</sup> by defining the *primer vector*,  $\mathbf{P} = -\mathbb{B}^\top \boldsymbol{\lambda}$ . This leads to the optimal thrust direction unit vector

$$\hat{\mathbf{P}}^* = \frac{\mathbf{P}}{\|\mathbf{P}\|} = -\frac{\mathbb{B}^\top \boldsymbol{\lambda}}{\|\mathbb{B}^\top \boldsymbol{\lambda}\|}. \quad (12)$$

Similarly, PMP is used to characterize the optimal throttling input as

$$\delta^* = \arg \min_{0 \leq \delta \leq 1} H. \quad (13)$$

After substituting Eq. (12) into Eq. (10) and rearranging the terms, to determine  $\delta$  we need to minimize the term,

$$-\frac{T}{c} \left[ \frac{c \|\mathbb{B}^\top \boldsymbol{\lambda}\|}{m} + \lambda_m - 1 \right] \delta \rightarrow \min. \quad (14)$$

We can simplify our analysis by defining the term inside the parenthesis as a switching function

$$S \equiv \frac{c \|\mathbb{B}^\top \boldsymbol{\lambda}\|}{m} + \lambda_m - 1. \quad (15)$$

The optimal value of the throttling input,  $\delta^*$ , depends on the sign of the  $S$ ,

$$\delta^*(S) = \begin{cases} 1, & \text{if } S > 0, \\ 0, & \text{if } S < 0 \end{cases} = \frac{1}{2} [1 + \text{sign}(S)]. \quad (16)$$

### Hyperbolic Tangent Smoothing Function

The hyperbolic tangent smoothing function for any bounded control input is used to approximate the sign function as

$$\delta^*(S)_{\text{bang-bang}} \approx \delta^*(S, \rho) = \frac{1}{2} \left[ (\delta_l + \delta_u) + (\delta_u - \delta_l) \tanh \left( \frac{S}{\rho} \right) \right], \quad (17)$$

where  $\rho$  is the smoothing parameter (and  $0 \leq \rho \leq 1$  will be used as the continuation parameter for the numerical continuation procedure). Clearly, as  $\rho \rightarrow 0$ , the  $\tanh$  function approximates the sign function and therefore the optimal control necessary conditions are contained as the limiting case of a one-parameter family. The continuation procedure for the simulations performed for this paper ended once the value of  $\rho$  was less than  $1 \times 10^{-5}$ . For the problems considered in this paper, the optimal engine throttling input has a bang-bang time history that can be expressed using a sign function. Specifically, we have  $\delta_l = 0$ ,  $\delta_u = 1$ . Therefore, the smoothed engine throttle input becomes the smoothed step function.

$$\delta^*(S) = \frac{1}{2} [1 + \text{sign}(S)] \cong \delta^*(S, \rho) = \frac{1}{2} \left[ 1 + \tanh \left( \frac{S}{\rho} \right) \right]. \quad (18)$$

The advantage of using a smoothed switch function is purely numerical. As the parameter  $\rho$  is swept to increasingly smaller values, the switches become more abrupt, and approximate the true bang-bang control structure to a greater accuracy. In the early iterations when the trajectory is far from the final solution, abrupt changes in the acceleration can lead to prohibitive numerical convergence cost because we need to isolate to high precision all  $S = 0$  switch time(s) on each iterative trajectory. In the case that the trajectory may consist of many switches, this increases the overhead and if the  $S = 0$  switch times are poorly isolated, quasi-random errors are introduced near each control switch, which degrades the overall convergence severely.

The smoothing parameter allows the switches to occur continuously, ensuring numerical convergence on each iteration. Qualitatively, introducing the smooth switches allows existing adaptive integrators to “see the switch coming” and adapt step-size automatically while maintaining high precision. As  $\rho \rightarrow 0$  the switches become sharper and the solution on the previously converged  $\rho$  value is used to start the following iteration, through continuation. The smoothness of the switch function means that the dynamics are also smooth in the initial iterations, and this is important when using any integrator and also important for path approximation integrators such as Picard-Chebyshev. More details on the Picard-Chebyshev implementation will be presented in a later section.

For a fixed-time rendezvous problem, the final conditions can be written in the form of seven equality constraints,

$$\psi(\mathbf{x}(t_f), \lambda_m(t_f), t_f) = \begin{bmatrix} \mathbf{x}(t_f) - \mathbf{x}_T \\ \lambda_m(t_f) \end{bmatrix} = \mathbf{0}, \quad (19)$$

where subscript ‘T’ denotes the target MEEs. Let  $\mathbf{z} = [\mathbf{x}^\top, m, \boldsymbol{\lambda}^\top, \lambda_m]^\top$  denote the state/costate vector, then, we can write,

$$\dot{\mathbf{z}} = \mathbf{F} = \begin{bmatrix} \dot{\mathbf{x}} \\ \dot{m} \\ \dot{\boldsymbol{\lambda}} \\ \dot{\lambda}_m \end{bmatrix}, \quad (20)$$

where  $\hat{\mathbf{P}} = \hat{\mathbf{P}}^*$  and  $\delta = \delta^*(S, \rho)$  are used in the RHS of Eq. (20). Numerical integration of the equations of motion requires the full state/costate vector information at the initial time,  $t_0$ . However, only the state initial conditions are known, i.e.,  $\mathbf{x}(t_0) = \mathbf{x}_0$  and  $m(t_0) = m_0$ . Let  $\boldsymbol{\Upsilon}(t_0) = [\boldsymbol{\lambda}^\top(t_0), \lambda_m(t_0)]^\top$  denote the vector of unknown initial costates. The problem is to find  $\boldsymbol{\Upsilon}(t_0) = [\boldsymbol{\lambda}^\top(t_0), \lambda_m(t_0)]^\top$  such that Eq. (19) is satisfied. As a consequence, we have a TPBVP that requires a starting estimate  $\boldsymbol{\Upsilon}(t_0)$ .

## NUMERICAL ALGORITHM

In this section, we demonstrate the solution procedure for solving the TPBVP associated with fuel-optimal orbit transfer problem using an indirect optimization method that combines the MPS with a single-shooting scheme. The integrator used for propagating the equations is the Picard-Chebyshev method.

### Picard-Chebyshev Numerical Integration

Picard-Chebyshev iteration differs from the well-known step integrators, such as Gauss-Jackson and Runge-Kutta, in that it is a *path approximation* numerical integrator rather than a *step-by-step* integrator. Long state trajectory arcs are approximated continuously in time and are updated at all time instances on each iteration.

The technique combines Picard iteration with the orthogonal Chebyshev polynomials. Emile Picard observed that any first order differential equation

$$\frac{d\mathbf{x}(t)}{dt} = \mathbf{f}(t, \mathbf{x}(t)), \quad t \in [t_0, t_f], \quad (21)$$

with an initial condition  $\mathbf{x}(t_0) = \mathbf{x}_0$  and any integrable right hand side may be rearranged, without approximation, to obtain the following integral equation:

$$\mathbf{x}(t) = \mathbf{x}(t_0) + \int_{t_0}^t \mathbf{f}(\tau, \mathbf{x}(\tau)) d\tau. \quad (22)$$

Picard further proposed that a sequence of approximate solutions  $\mathbf{f}^i(t)$ , ( $i = 1, 2, 3, \dots, \infty$ ), of the true solution  $\mathbf{x}(t)$  that satisfies this differential equation may be obtained through Picard iteration using the following Picard sequence of approximate paths  $\{\mathbf{x}^0(t), \mathbf{x}^1(t), \dots, \mathbf{x}^{i-1}(t), \mathbf{x}^i(t), \dots\}$ :

$$\mathbf{x}^i(t) = \mathbf{x}(t_0) + \int_{t_0}^t \mathbf{f}(\tau, \mathbf{x}^{i-1}(\tau)) d\tau, \quad i = 1, 2, \dots \quad (23)$$

Picard proved that for smooth, differentiable, single-valued nonlinear functions  $\mathbf{f}(t, \mathbf{x}(t))$ , there is some maximum time interval  $|t_f - t_0| < d$  and a starting trajectory  $\mathbf{x}^0(t)$  that satisfies the following condition:  $\|\mathbf{x}^0(t) - \mathbf{x}(t)\|_\infty < \Delta$ . For suitable finite bounds ( $d, \Delta$ ), the Picard sequence of trajectories represents a contraction operator that converges to the unique solution of the initial value problem. There is a literature<sup>34,35</sup> that deals with approximating ( $d, \Delta$ ). These convergence bounds are typically quite large in astrodynamics, where  $d$  can be up to three low Earth orbit periods in Cartesian coordinates and over ten orbit periods in MEEs.<sup>36</sup> Although the convergence domain is large, it is not efficient to use such large segments and the trajectory is divided into multiple time segments that are patched together head-to-tail. The rate of convergence is typically geometric. The guaranteed convergence property sets the Picard-Chebyshev method apart from other integration methods. The numerical accuracy and efficiency are dominated by the particular process used to carry out the integral; note since the previous ( $i - 1$ ) trajectory approximation is known, the integrand is considered a function of time only. Chebyshev polynomials are used for approximating the integrand in the Picard iteration sequence, and these orthogonal polynomials integrate to produce a Chebyshev series for the integral, including the imposition of initial (or final) boundary conditions.

Picard-Chebyshev requires smooth functions that are twice differentiable. For the case of on-off thrust the acceleration is not continuous/smooth and accurate propagation over the discontinuous acceleration step input is a challenge for Picard-Chebyshev. To overcome this problem, we compute the segment break times by numerically solving for the zeros of the switch function, thus allowing us to strategically place segment breaks at the on/off thrust boundaries.

It is important that the hyperbolic tangent smoothing version of the switch function passes through zero at exactly  $S = 0$ . After each MPS iteration the switch function is sampled on a cosine distribution and fit with Chebyshev polynomials. The closest node on each side of the zero (one positive and one negative) is used to start a secant method to solve for the value of  $\tau$  (accurate to 13 digits) corresponding to  $S = 0$ . The secant method can be thought of as a “finite difference” version of Newton’s method and thus requires two initial times to get started. We can also use a Newton method, since  $ds/dt$  is easily computed analytically, however, the secant method converges very

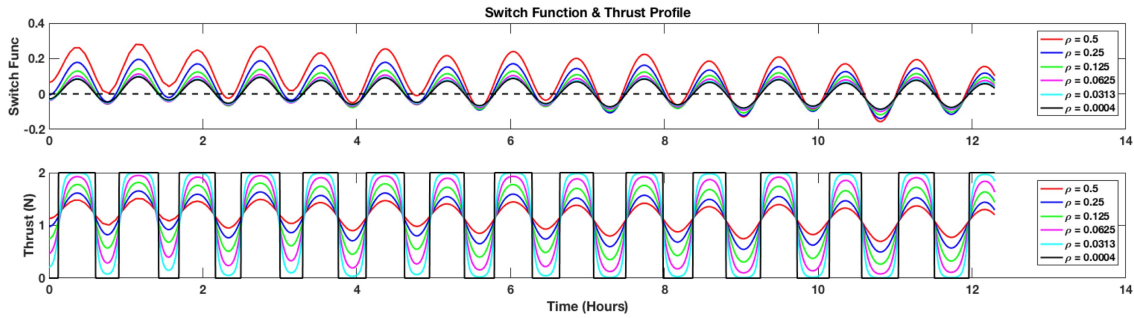


**Figure 1. An example of continuation on the switch function and thrust profile for a low thrust orbit transfer between two low Earth orbits.**

rapidly (usually in 2 or 3 iterations.) The converged  $\tau$  value is converted to a time which is set as a segment boundary in the next set of Picard-Chebyshev iterations.

As the value of  $\rho$  is reduced, through continuation (see Figure 1), the hyperbolic tangent function approaches a step function and the thrusting profile approaches a “bang-bang” profile. The bang-bang profile is certainly not smooth or continuous, however, the segment break points from the previous MPS iteration are already in the vicinity of the switch, where the nodal density is high, and so even if the precomputed switches are slightly shifted from the actual thrust arc on the current iteration, the dynamics are still well approximated and the method converges. This method works very well for thrust values in the range ( $0 \leq T \leq 2$  N) where the abrupt changes in the acceleration are small in magnitude, however for problems that require larger thrust magnitudes step-by-step integrators may be a better choice.

The original fusion of orthogonal approximation theory and Picard iteration was introduced by Clenshaw and Norton in 1963.<sup>37</sup> Feagin published his PhD dissertation<sup>38</sup> in 1972 on Picard iteration using Chebyshev approximation. He established the first vector-matrix version of Picard iteration utilizing orthogonal basis functions.<sup>39</sup> In 1980 Shaver wrote a related dissertation giving insights on parallel computation using Picard Iteration and Chebyshev approximation.<sup>40</sup> In 1997 Fukushima<sup>41</sup> addressed parallelization of Picard iteration in a particular computer architecture. His results showed that a particular parallel implementation of his algorithm did not give the theoretical speedup he anticipated.

A decade later Bai and Junkins revisited this approach and developed improved algorithms for solving initial value problems (IVPs) and TPBVPs.<sup>42,43</sup> They established new convergence insights and also developed vector-matrix formulations for solving initial and boundary value problems. These are published in Bai’s PhD dissertation.<sup>44</sup> Bani Younes and Junkins followed this work with methods to include high-order gravity perturbations to more accurately represent the motion of satellites orbiting in the vicinity of the Earth.<sup>45–48</sup> Macomber and Junkins developed enhancements that took advantage of the “fixed-point” convergence nature of Picard-Chebyshev iteration and allowed solutions to the perturbed two-body problem to be computed using variable-fidelity force models and radially adaptative gravity approximations. They also made use of *warm* and *hot* starts for solving the perturbed problem.<sup>49,50</sup> These enhancements resulted in substantial increases in the efficiency of Picard-Chebyshev while maintaining machine precision accuracy. Junkins and Woolands built on this work to develop an accelerated and adaptive (self-tuning), Picard-Chebyshev algorithm for solution of the perturbed two-body problem.<sup>51,52</sup>

## Method of Particular Solutions

MPS differs from the well-known analytic state transition matrix (STM) method in that integration of the STM is not required. The STM integration involves 196 additional differential equations that have to be propagated. Instead, MPS relies on the assumption of local linearity and makes iterative differential corrections using a reference trajectory and a linear combination of the relative displacements of the  $n$  particular solutions. In addition and unlike the STM method, the trajectory does not need to be *continuous*.

MPS can be used to solve a TPBVP with any combination of unknown initial and final boundary conditions. The following derivation is general in the sense that the initial costates are iteratively updated to hit the desired final states. Similarly MPS may be used to iteratively update the initial velocity to satisfy the desired final position when solving the perturbed Lambert's problem.<sup>29,53</sup> For the minimum-fuel optimal control problem with free final mass ( $m(t_f)$ ), we also have a known zero final boundary condition  $\lambda_m$ , and this along with the final state boundary conditions are enforced during the MPS iterations.

Consider the state and costate differential equations

$$\begin{Bmatrix} \dot{\mathbf{x}} \\ \dot{\boldsymbol{\lambda}} \end{Bmatrix} = \begin{Bmatrix} \mathbf{G}(t, \mathbf{x}(t), \boldsymbol{\lambda}(t)) \\ \mathbf{Q}(t, \mathbf{x}(t), \boldsymbol{\lambda}(t)) \end{Bmatrix}, \quad (24)$$

where  $\mathbf{x} = [p, f, g, h, k, l, m]^\top$  and  $\boldsymbol{\lambda} = [\lambda_p, \lambda_f, \lambda_g, \lambda_h, \lambda_k, \lambda_l, \lambda_m]^\top$ . MPS makes use of a reference trajectory  $\mathbf{x}_{\text{ref}}(t)$ ,  $\boldsymbol{\lambda}_{\text{ref}}(t)$  and all neighboring solutions of Eq. (24) can be re-formulated exactly in terms of a departure motion  $\Delta\mathbf{x}(t)$ ,  $\Delta\boldsymbol{\lambda}(t)$  as

$$\mathbf{x}(t) = \mathbf{x}_{\text{ref}}(t) + \Delta\mathbf{x}, \quad \dot{\mathbf{x}}(t) = \dot{\mathbf{x}}_{\text{ref}}(t) + \Delta\dot{\mathbf{x}}, \quad (25)$$

$$\boldsymbol{\lambda}(t) = \boldsymbol{\lambda}_{\text{ref}}(t) + \Delta\boldsymbol{\lambda}, \quad \dot{\boldsymbol{\lambda}}(t) = \dot{\boldsymbol{\lambda}}_{\text{ref}}(t) + \Delta\dot{\boldsymbol{\lambda}}. \quad (26)$$

From Eq. (25) and Eq. (24), we can write the exact departure motion differential equation:

$$\begin{Bmatrix} \Delta\dot{\mathbf{x}} \\ \Delta\dot{\boldsymbol{\lambda}} \end{Bmatrix} = \begin{Bmatrix} \mathbf{G}(t, \mathbf{x}_{\text{ref}}(t) + \Delta\mathbf{x}, \boldsymbol{\lambda}_{\text{ref}}(t) + \Delta\boldsymbol{\lambda}) \\ \mathbf{Q}(t, \mathbf{x}_{\text{ref}}(t) + \Delta\mathbf{x}, \boldsymbol{\lambda}_{\text{ref}}(t) + \Delta\boldsymbol{\lambda}) \end{Bmatrix} - \begin{Bmatrix} \dot{\mathbf{x}}_{\text{ref}}(t) \\ \dot{\boldsymbol{\lambda}}_{\text{ref}}(t) \end{Bmatrix}. \quad (27)$$

Now consider the circumstance that  $\dot{\mathbf{x}}_{\text{ref}}(t)$ ,  $\dot{\boldsymbol{\lambda}}_{\text{ref}}(t)$  is a solution of the differential equation, which satisfies "good" initial boundary conditions, in this case, the  $\Delta$ 's can be expected to be small,  $\dot{\mathbf{x}}_{\text{ref}}(t) = \mathbf{G}(t, \mathbf{x}_{\text{ref}}(t), \boldsymbol{\lambda}_{\text{ref}}(t))$ ,  $\dot{\boldsymbol{\lambda}}_{\text{ref}}(t) = \mathbf{Q}(t, \mathbf{x}_{\text{ref}}(t), \boldsymbol{\lambda}_{\text{ref}}(t))$  and to a linear approximation, the exact nonlinear Eq. (27) could be replaced by an approximate linear equation of the form

$$\begin{Bmatrix} \Delta\dot{\mathbf{x}} \\ \Delta\dot{\boldsymbol{\lambda}} \end{Bmatrix} = \mathbb{A} \begin{Bmatrix} \Delta\mathbf{x} \\ \Delta\boldsymbol{\lambda} \end{Bmatrix} + O(\Delta^2). \quad (28)$$

where  $\mathbb{A}$  is the time varying Jacobian of  $\mathbf{G}$  and  $\mathbf{Q}$  with respect to  $\mathbf{x}$  and  $\boldsymbol{\lambda}$  evaluated along  $\mathbf{x}_{\text{ref}}(t)$  and  $\boldsymbol{\lambda}_{\text{ref}}(t)$ . To within the accuracy that the linear terms of Eq. (28) approximate the exact departure motion of Eq. (27), we can consider that the departure motion is linear. Consider also the case that the reference motion satisfies the known left boundary elements exactly  $\mathbf{x}_{\text{ref}}(t_0) = \mathbf{x}_0$ , and the initial costates  $\boldsymbol{\lambda}_{\text{ref}}(t_0)$  represents the current best estimate of the unknown initial costates. In this paper,

we select  $n = 7$  as there are seven unknown initial costates  $(\lambda_p, \lambda_f, \lambda_g, \lambda_h, \lambda_k, \lambda_l, \lambda_m)$  that we wish to determine. For this given (or just computed)  $\mathbf{x}_{\text{ref}}(t)$ , consider  $n$  neighboring variant trajectories obtained by varying the initial costates by small linearly independent perturbations.

$$\mathbf{x}_j(t_0) = \mathbf{x}_{\text{ref}}(t_0) = \mathbf{x}_0, \quad \boldsymbol{\lambda}_j(t_0) = \boldsymbol{\lambda}_{\text{ref}}(t_0) + \Delta\boldsymbol{\lambda}_j(t_0), \quad j = 1, 2, \dots, n. \quad (29)$$

Now solve the differential Eq. (24) for each of the  $n$  particular solutions  $\mathbf{x}_j(t)$ ,  $\boldsymbol{\lambda}_j(t)$ . We can compute the exact departure motions

$$\Delta\mathbf{x}_j(t) = \mathbf{x}_j(t) - \mathbf{x}_{\text{ref}}(t). \quad (30)$$

These exact departure motions are particular solutions and conjectured to approximately satisfy the linear differential equation in Eq. (28). Since independent costate initial conditions were used, it is assumed that these trajectories span the space of interest along with all neighboring trajectories of interest that also satisfy the linear departure motion Eq. (28). The linear combination of any particular solution of a linear differential equation satisfies the differential equation as well, and the general solution as a linear combination of  $n$  departure motions can be written in the form:

$$\Delta\mathbf{x}(t) \approx \sum_{j=1}^n \alpha_j \Delta\mathbf{x}_j(t) \Rightarrow \mathbf{x}(t) \approx \mathbf{x}_{\text{ref}}(t) + \sum_{j=1}^n \alpha_j \Delta\mathbf{x}_j(t). \quad (31)$$

$$\boldsymbol{\lambda}(t) = \boldsymbol{\lambda}_{\text{ref}}(t) + \sum_{j=1}^n \alpha_j \Delta\boldsymbol{\lambda}_j(t). \quad (32)$$

Evaluating Eq. (31) at the final time and imposing the desired result that  $\mathbf{x}(t_f) = \mathbf{x}_f$ , leads to the solution for the coefficients of linear combination

$$\begin{Bmatrix} \alpha_1 \\ \vdots \\ \alpha_n \end{Bmatrix} \approx [ \Delta\mathbf{x}_1(t_f) \quad \dots \quad \Delta\mathbf{x}_n(t_f) ]^{-1} \{ \mathbf{x}(t_f) - \mathbf{x}_{\text{ref}}(t_f) \}. \quad (33)$$

Given the  $\alpha_i$ s, we can compute the departure  $\Delta\mathbf{x}(t)$  and  $\Delta\boldsymbol{\lambda}(t)$  at any time  $t$ .

$$\Delta\mathbf{x}(t_f) = \alpha_1 \Delta\mathbf{x}_1(t_f) + \dots + \alpha_n \Delta\mathbf{x}_n(t_f), \quad (34)$$

$$\Delta\boldsymbol{\lambda}(t_f) = \alpha_1 \Delta\boldsymbol{\lambda}_1(t_f) + \dots + \alpha_n \Delta\boldsymbol{\lambda}_n(t_f). \quad (35)$$

The costate departure equation obviously holds at time  $t_0$ , so the time derivative of Eq. (33), evaluated at time  $t_0$ , allows a new estimate for the initial costates to be calculated.

$$\boldsymbol{\lambda}_{\text{new}}(t_0) = \boldsymbol{\lambda}_{\text{ref}}(t_0) + \sum_{j=1}^n \alpha_j \Delta\boldsymbol{\lambda}_j(t_0). \quad (36)$$

Given an invertible matrix in Eq. (33), Eq. (24) can now be re-solved with the reference trajectory's initial costate replaced by  $\boldsymbol{\lambda}_{\text{new}}(t_0)$ . We iterate for improved values of  $\alpha$  using Eqs. (33) and (36), analogous to Newton's method, but without the necessity of solving the STM to obtain the partials  $\frac{\partial \mathbf{x}(t_f)}{\partial \boldsymbol{\lambda}_0}$ .

## Local Force Approximations

Any numerical integrator can be used for solving TPBVPs with the MPS. However, using Picard-Chebyshev affords an avenue for increased efficiency that is not available with other step-by-step integrators. The two key features of this method that make it unique with respect to other TPBVP solvers are, first, Picard-Chebyshev is a path approximation numerical integrator, and second, the particular solutions lie close to the reference trajectory. As a first consequence, the current trajectory is a hot start for all neighboring particular solutions of the MPS approach.

The path approximation nature of the MPS means that at each Picard iteration the Chebyshev nodes along the trajectory are being updated and are converging towards fixed points in space. The fact that during terminal convergence the Picard iteration solutions lie so close to converged reference trajectory (within the linear domain) means that each node along the iterative solutions converges to a fixed point in space that is very close to the location of the converged node on the reference trajectory. These comments also apply, approximately to the neighboring particular solutions of the MPS approach.

We know from previous studies<sup>50–52</sup> that the gravity gradient is constant to greater than 9 digits within 50 meters of a converged node. As a result, it is not necessary to call the full, computationally expensive, gravity model when computing the particular solutions. Instead we can use local force approximations, with respect to the reference trajectory, that significantly accelerate the computational efficiency without loss of accuracy. Woollands et al.<sup>53</sup> utilized a similar approach for solving the perturbed Lambert’s problem with MPS and Picard-Chebyshev iteration.

Let  $\mathbf{a}_{2B}$  denote the two-body acceleration vector, the high-fidelity (*full*) and low-fidelity (*low*) accelerations vectors computed at each of the nodes along the reference trajectory are denoted as

$$\mathbf{a}_{full_{ref}} = \mathbf{a}_{(70 \times 70)} \text{ spherical harmonic gravity}, \quad (37)$$

$$\mathbf{a}_{low_{ref}} = \mathbf{a}_{2B_{ref}} + \mathbf{a}_{(J_2+J_3+J_4+J_5+J_6)_{ref}}. \quad (38)$$

The acceleration offset ( $\Delta \mathbf{a}$ ) between the high- and low-fidelity models on the reference trajectory is given by

$$\Delta \mathbf{a} = \mathbf{a}_{full_{ref}} - \mathbf{a}_{low_{ref}}. \quad (39)$$

Since the particular solutions are assumed to remain close to the reference trajectory, their accelerations may be approximated (without calling the full force model) at any node using Eq. (40).

$$\mathbf{a}_{approx_{particular}} = \mathbf{a}_{2B_{particular}} + \mathbf{a}_{(J_2+J_3+J_4+J_5+J_6)_{particular}} + \Delta \mathbf{a}. \quad (40)$$

Remarkably, we demonstrate that computing the seven particular solutions with only low-fidelity approximate gravity function evaluations, that is, *two-body plus zonal perturbations plus the difference between the full force evaluation and two-body plus zonal perturbations on the reference trajectory*, greatly increases the efficiency of the algorithm while maintaining near-machine precision accuracy. Qualitatively, this is because the resulting corrections are continuously to the right, most four or fewer significant digits, and the approximate gravity gives  $\Delta \lambda_j(t_0)$  that contribute to four or fewer digits in the terminal iterations. In the following section we show that solving the the fuel-optimal transfer problem using MPS with Picard-Chebyshev iteration requires about an order of magnitude fewer function evaluations than the classical single-shooting method.

Costate differential equations are derived by applying the Euler-Lagrange equation, i.e., taking partial derivatives of the Hamiltonian with respect to each of the states (multiplied by negative one).

This is achieved through an automated code (using MATLAB’s symbolic toolbox) that has been developed and used extensively in previous works.<sup>25–27</sup> The complexity of the costate differential equations can vary depending on the fidelity of the gravity model required for propagating the state equations.

In this paper, we consider a  $70 \times 70$  degree and order spherical harmonic gravity model for propagating the state equations. Deriving the costate equations with this high-fidelity gravity model is time consuming (even with a symbolic manipulator) and leads to long expressions that are numerically expensive to evaluate and solve. Depending on the complexity of the state dynamics, generation of the algebraic expressions that describe costate dynamics may take a couple of hours (or more). As a consequence, a reduced-order force model (two-body plus the disturbing accelerations due to  $J_2$  through  $J_4$  zonal harmonic terms) is used for deriving the costate differential equations. Note that we still consider a high-fidelity force model in the state differential equations.

Some of the important relations that are required for implementing  $J_2$  to  $J_4$  zonal harmonics are explained for clarity. The components of the acceleration due to  $J_2$ ,  $J_3$  and  $J_4$  (when expressed in the LVLH frame) are given<sup>54</sup>

$$\mathbf{a}_{J_2} = \begin{bmatrix} -\frac{3\mu J_2 R^2}{2r^4} (1 - 3s_i^2 s_\theta^2) \\ -\frac{3\mu J_2 R^2}{r^4} s_i^2 s_\theta c_\theta \\ -\frac{3\mu J_2 R^2}{r^4} s_i c_i s_\theta \end{bmatrix}, \quad \mathbf{a}_{J_3} = \begin{bmatrix} -\frac{\mu J_3 R^2}{r^5} [6s_i c_\theta - \frac{5}{2} s_i^3 (3s_\theta - s_{3\theta})] \\ -\frac{\mu J_3 R^2}{2r^5} [\frac{15}{4} s_i^3 (c_\theta - c_{3\theta}) - 3s_i c_\theta] \\ -\frac{\mu J_3 R^2}{2r^5} [\frac{15}{2} s_i^2 c_i (1 - c_{2\theta}) - 3c_i] \end{bmatrix}$$

$$\mathbf{a}_{J_4} = \begin{bmatrix} -\frac{5\mu J_4 R^4}{8r^6} [15s_i^2 (1 - c_{2\theta}) - \frac{35}{8} s_i^4 (3 - 4c_{2\theta} + c_{4\theta}) - 3] \\ -\frac{5\mu J_4 R^2}{2r^6} [\frac{7}{4} s_i^4 c_\theta (3s_\theta - s_{3\theta}) - 3s_i^2 s_\theta c_\theta] \\ -\frac{5\mu J_4 R^2}{2r^6} [\frac{7}{4} s_i^3 c_i (3s_\theta - s_{3\theta}) - 3s_i c_i s_\theta] \end{bmatrix},$$

where  $s_{n\theta} = \sin(n\theta)$ ,  $c_{n\theta} = \cos(n\theta)$ ,  $s_i = \sin(i)$  and  $c_i = \cos(i)$ . In addition, the classical elements inclination,  $i$ , and true anomaly  $\theta$  are related to  $p$ ,  $q$ ,  $l$ .<sup>55</sup> It is also possible to express the terms in parentheses (e.g,  $(3 - 4c_{2\theta} + c_{4\theta})$  in terms of  $s_\theta$  and  $c_\theta$ ) in terms of the existing relations. Ultimately, the perturbing accelerations can be expressed entirely as a function of MEEs.

Since solution of the costate equations determines the optimal control, using a lower-fidelity model in the costate equations will only effect the degree of “optimality” attainable by the algorithm. As long as the state equations contain the high-fidelity force model, the solution will accurately represent the orbit dynamics but with a slightly reduced performance (marginally sub-optimal) for making the maneuver. We investigate how including various zonal perturbations ( $J_2$  through  $J_4$ ) affects the final mass, and we find that typically engineering precision for the optimal control is obtained.

## OPTIMAL ORBIT TRANSFER EXAMPLES

We demonstrate the performance of our algorithm by solving fuel-optimal trajectories between four sets of boundary conditions in a fixed time-of-flight. The initial and final MEEs are given in Table 1. In all cases the initial spacecraft mass is 100 kg, the maximum allowable thrust magnitude is 2 N, and the specific impulse of the propulsion system is 3000 seconds. We use a  $70 \times 70$  degree and order spherical harmonic gravity model for propagating the orbit equations of motion, and test several lower-fidelity gravity models in the costate equations, from two-body through to the fourth zonal harmonic ( $J_2 = 1082.63 \times 10^{-6}$ ,  $J_3 = -2.52 \times 10^{-6}$ ,  $J_4 = -1.61 \times 10^{-6}$ ).

**Table 1. Initial and final conditions for the four test case orbits.**

		$p (R_{\oplus})$	$f$	$g$	$h$	$k$	$l$ (rad)	$m(t_0)$ (kg)	$t$ (hours)
Case 1	Initial	1.060	0.010	0	0.254	0	0	100	0
	Final	1.159	0.010	0.006	0.253	0.001	35.221	free	9.221
Case 2	Initial	1.060	0.010	0	0.613	0	0	100	0
	Final	1.159	0.010	0.005	0.612	0.001	35.221	free	9.221
Case 3	Initial	1.100	0.010	0	1.091	0	0	100	0
	Final	1.212	0.010	0.006	1.090	0.003	35.041	free	9.747
Case 4	Initial	1.200	0.010	0	0.044	0	0	100	0
	Final	1.346	0.012	0.007	0.043	0.002	34.560	free	11.106

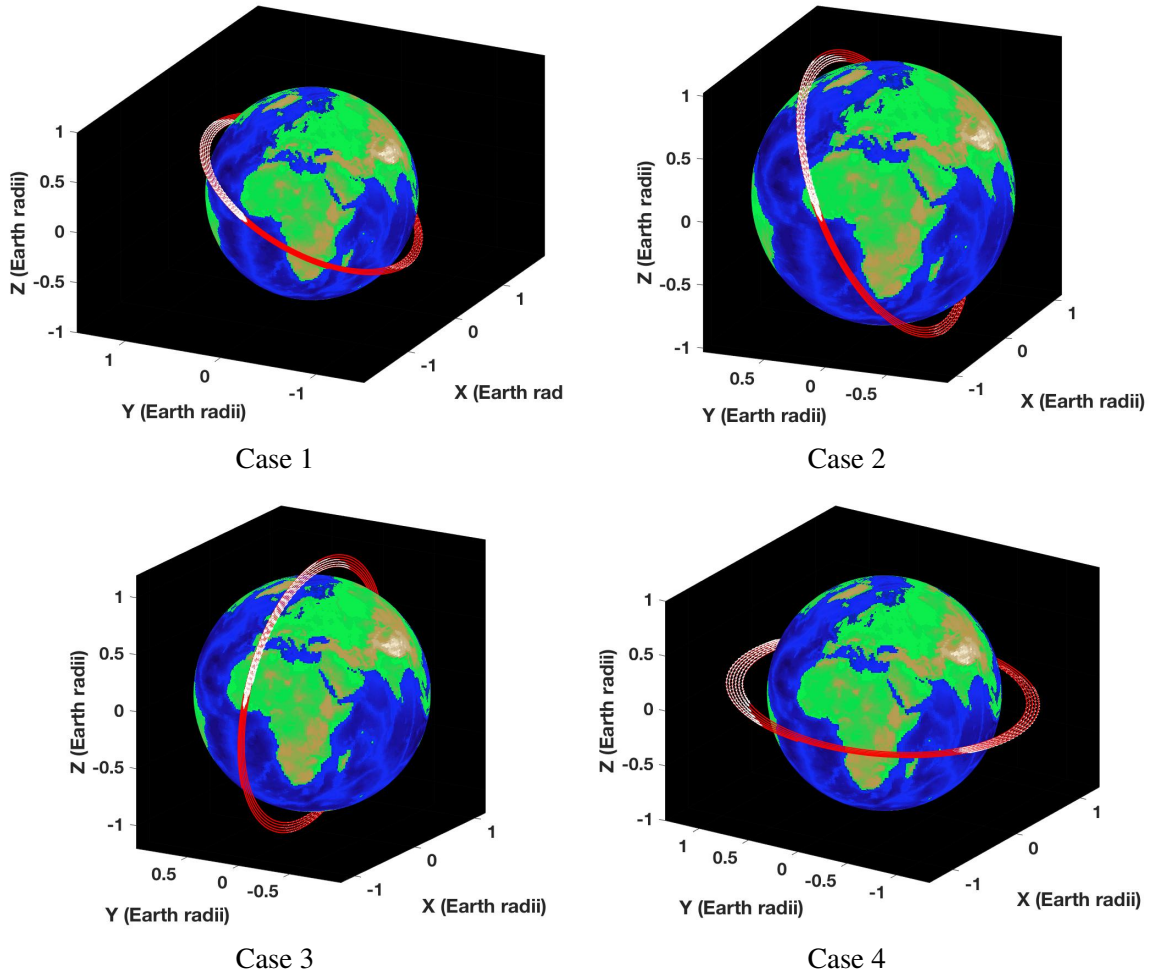


**Figure 2. Low thrust orbit spirals for the four test cases presented in Table 1.**

Figure 2 shows the optimal transfer trajectory for the four test case orbits summarized in Table 1, where the white arrows represent the instantaneous thrust vector. Figures 3 and 4 show the time histories of the six MEEs and the corresponding costates for Case 1. The mass and mass costate time histories are shown in the left panel of Figure 5, and the switch function and thrust profile are shown in the right panel. The final value of the costate associated with mass converges to zero.

Lawden's primer vector determines the optimal direction of thrusting. However, the time history of the switch function automatically determines when thrust and coast arcs should occur to ensure optimality. When the switch function is positive the thruster is switched on to the maximum thrust level ( $T = 2$  N), and when the switch function is negative the thrust is off.

Note that the switch function is plotted with circles that clearly reveal the clustering of Chebyshev nodes, by design, near the on/off switch points, which also correspond to the segment break times. Twelve thrust arcs and twelve coast arcs are required for completing the optimal orbit transfer, which raise the semimajor axis by 629 km in about 9.2 hours.

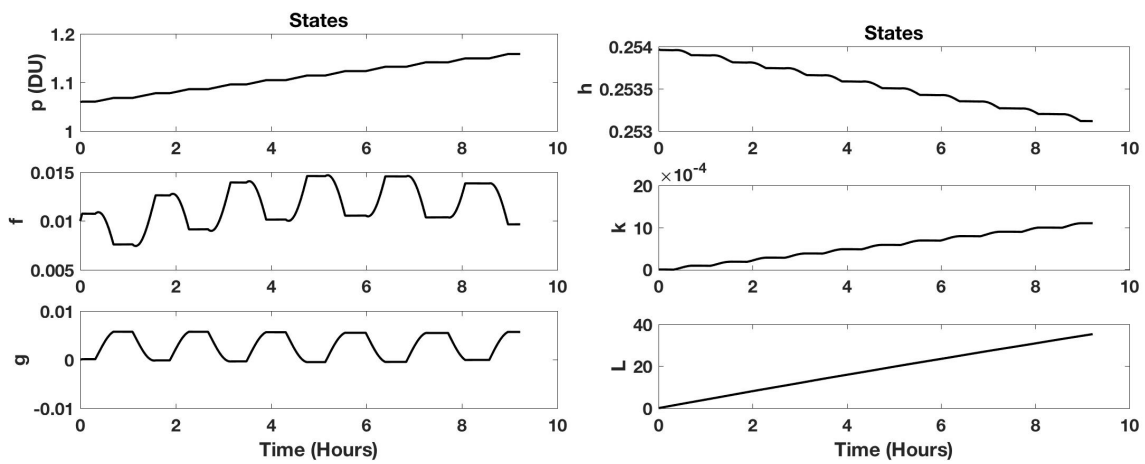


Figure 3. Time histories of MEEs for Case 1.

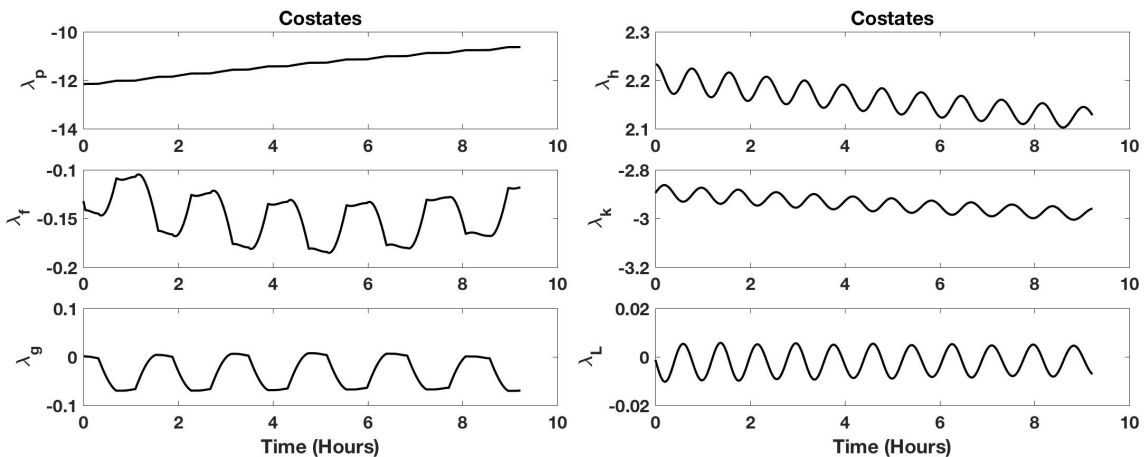
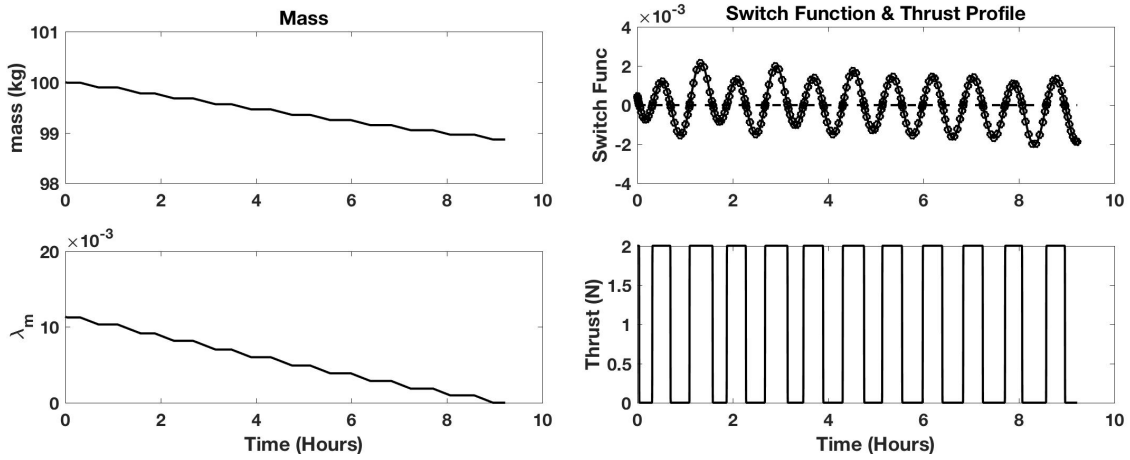


Figure 4. Time history of costates associated with the MEEs for Case 1.

Figures 6, 7 and 8 show the time histories of the states, costates, mass, switch function and thrust



**Figure 5. Mass and its corresponding costate time histories (left), and switch function and its corresponding thrusting profile (right) for Case 1.**

for Case 2, which has the same starting orbit as Case 1 but with a greater inclination. The optimal transfer consists of twelve coast arcs and eleven thrust arcs. Further notice, the control appears graphically to switch instantaneously, although the control is mathematically smooth. Moreover, the thrust profile indicates that the transfer has initial and final coast arcs. The existence of late-departure and early-arrival phenomena is discussed in details in.<sup>56</sup> Taheri and Junkins have shown in<sup>56</sup> that the combination of the prescribed boundary conditions along with the chosen time of flight and engine parameters lead to this situation. These boundary coast intervals usually occur when the existing thrust magnitude is a large value. As a consequence of the extra thrust (and its ensuing acceleration), the spacecraft remains on the initial orbit for some time interval and then fires its engine at an appropriate time instant, which is determined through optimality criteria. Similarly, the spacecraft merges into the final orbit at a time earlier than what has been prescribed as the final time,  $t_f$ . If the final boundary conditions represented a target body, the existence of early-arrival condition means that the spacecraft has established a rendezvous status (i.e., the velocity and position vectors of the spacecraft and target body match) earlier than the prescribed final time. Note that the existence and introduction of terminal coast phases is a standard approach for improving an existing impulsive solution.<sup>57</sup> On the other hand, as the thrust magnitude is increased, the duration of thrust arcs get smaller. Eventually, infinite instantaneous thrust approximates the velocity impulses. These impulsive maneuvers frequently consist of late-departure and early-arrival coast boundaries.

Table 2 shows the final mass of the spacecraft using different models for the costate equations. The first row in the table shows the simulation results for the four test cases, using a  $70 \times 70$  degree and order spherical harmonic gravity model for the dynamic equations and a two-body model for the costate equations. The second, third and fourth rows show the final spacecraft mass upon arrival, using a  $70 \times 70$  degree and order spherical harmonic gravity model for the dynamic equations and inclusion of various zonal perturbations in the costate model. The zonal perturbations in the costate equations are computed analytically as described earlier. The results indicate that as higher order terms are included, the final mass decreases. However, it is clear from these simulations and results that taking into account the perturbing acceleration due to the third and fourth zonal harmonics in the costate equations affects the amount of fuel used at the milligrams level or less. This suggests that we have already reached the point of diminishing returns. Several of the tesseral

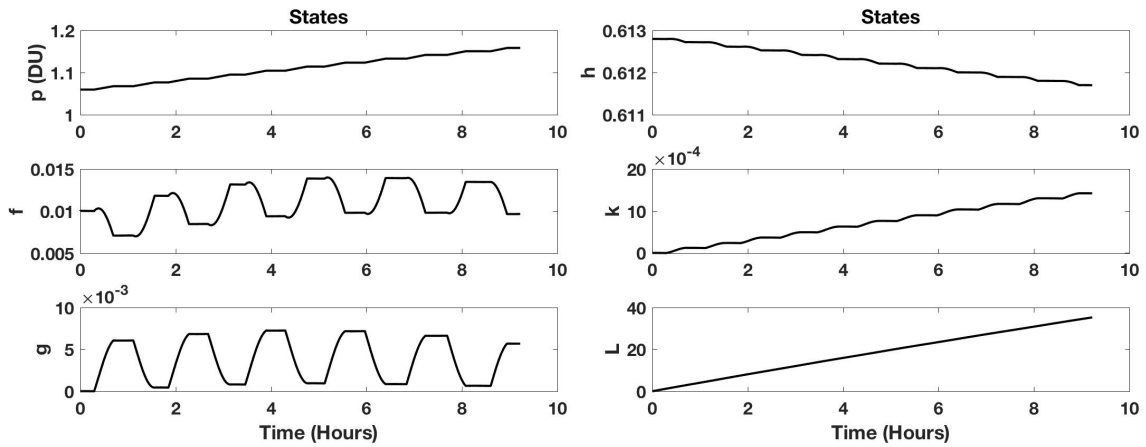


Figure 6. Time histories of the MEEs for Case 2.

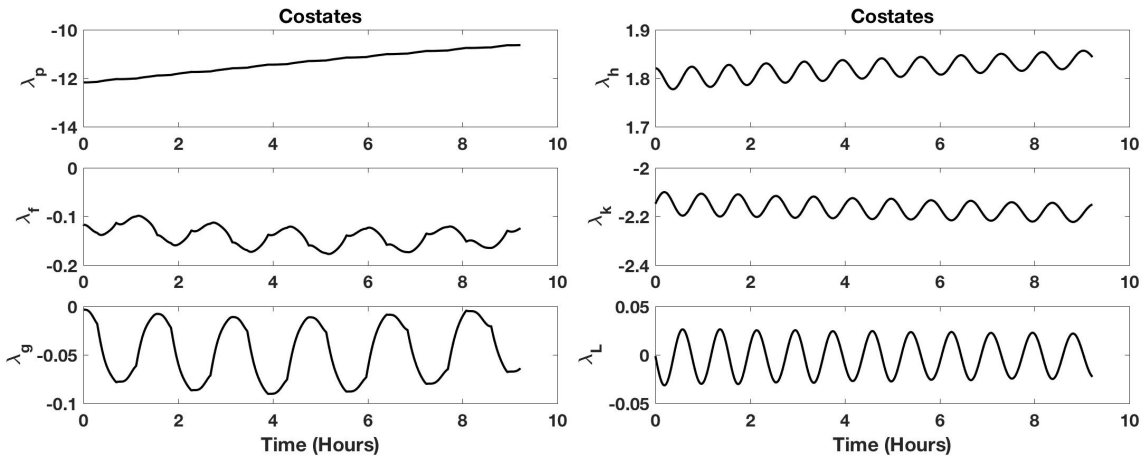


Figure 7. Costate time histories associated with the MEEs for Case 2.

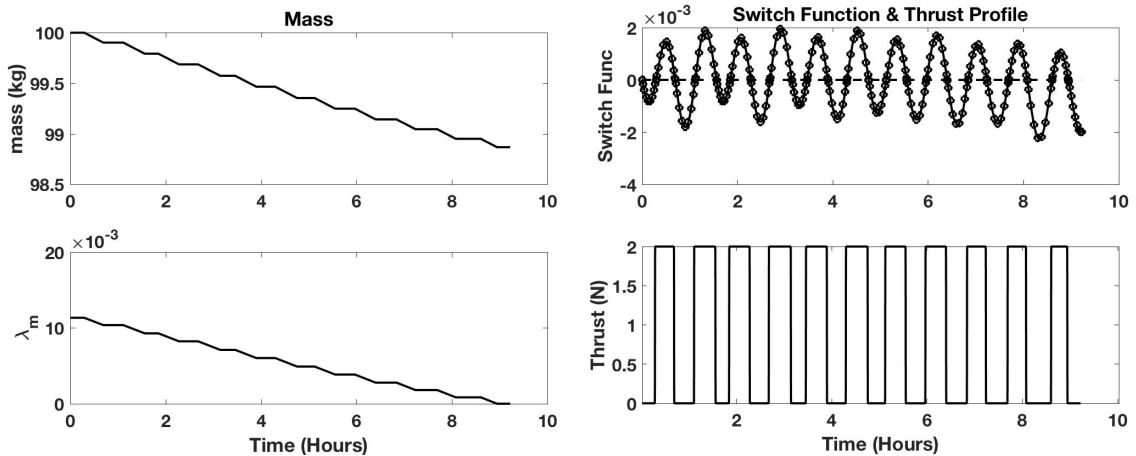


Figure 8. Mass and its corresponding costate time histories (left), and switch function and its corresponding thrusting profile (right) for Case 2.

and sectorial harmonics are comparable to  $J_3$  and  $J_4$ , it is likely that the full gravity field will affect the fuel consumed in the 8<sup>th</sup> or higher significant figure. These remarks appear to hold for a small number of revolutions and for the non-resonant cases. Using analogous computations, this approach provides insight to mission designers that is useful for determining what fidelity costate model to use depending on the accuracy of the optimality required for mission design purposes.

We should mention that Kechichian<sup>54</sup> had performed a similar analysis for time-optimal transfers from a low-Earth orbit to the geostationary Earth orbit using a relatively high constant thrust acceleration. The ensuing transfer takes place over a short time interval during which the spacecraft experiences very little zonal perturbation effects. Therefore, the net result between the case when  $J_2$  is considered and the case when  $J_2$  up to  $J_4$  are considered is negligible (which reflect itself in minor differences between the final true longitude at the insertion point to the GEO orbit). However, accumulation of the effects of zonal harmonics will have a greater impact on the time of flight on multi-revolution low-thrust trajectories as is shown for time-optimal maneuvers.<sup>58</sup> A similar impact on the final delivered mass is predictable for long multi-revolution fuel-optimal trajectories. Also long-spiral resonant transfer cases where the target orbit period becomes an bears an integer relationship to  $\frac{2\pi}{24 \text{ hours}}$  require special attention.

**Table 2. Final spacecraft mass for different gravity models used for deriving costate dynamics.**

Gravity Model	$m_f$ (kg)			
	Case 1	Case 2	Case 3	Case 4
Two-body	98.86720 <b>7529</b>	98.8671 <b>48693</b>	98.8026 <b>67679</b>	98.635 <b>625919</b>
Two-body + $J_2$	98.867203 <b>666</b>	98.867133 <b>484</b>	98.802650 <b>475</b>	98.63554 <b>1013</b>
Two-body + $J_2+J_3$	98.867203 <b>411</b>	98.867133 <b>410</b>	98.802650 <b>663</b>	98.635544 <b>058</b>
Two-body + $J_2+J_3+J_4$	98.867203 <b>391</b>	98.867133 <b>396</b>	98.802650 <b>691</b>	98.635544 <b>452</b>

## CONCLUSION

We have presented a new method for solving the optimal low thrust minimum-fuel orbit transfer problem in the near vicinity of a large body (planet or asteroid), considering a high fidelity spherical harmonic gravity model for the state dynamics. The algorithm was formulated via the indirect variational calculus approach, leading to a two-point boundary value problem. As state variables, we used the modified equinoctial elements, and the corresponding initial costates were updated iteratively in order to converge to the target final state boundary conditions. We made use of a hyperbolic tangent smoothing law for performing continuation on the thrust magnitude to reduce the sharpness of the control switches in early iterations and thus promote efficient and accurate convergence. The two-point boundary value problem is solved using the method of particular solutions shooting method and Picard-Chebyshev numerical integration. Any integrator could be used for solving TPBVPs with the method of particular solutions, however we show that using Picard-Chebyshev integration affords an avenue for increased efficiency that is not available with step-by-step integrators. We demonstrate that computing the particular solutions with only a low fidelity force model greatly increases the efficiency of the algorithm while ultimately achieving near machine precision accuracy. We are confident that this new optimal low thrust transfer algorithm will have widespread use and applicability in the astrodynamics community. In particular, it would be very useful for trajectory design in the near vicinity of small asteroids and also for “traveling salesman problem” associated with orbit debris rendezvous and removal.

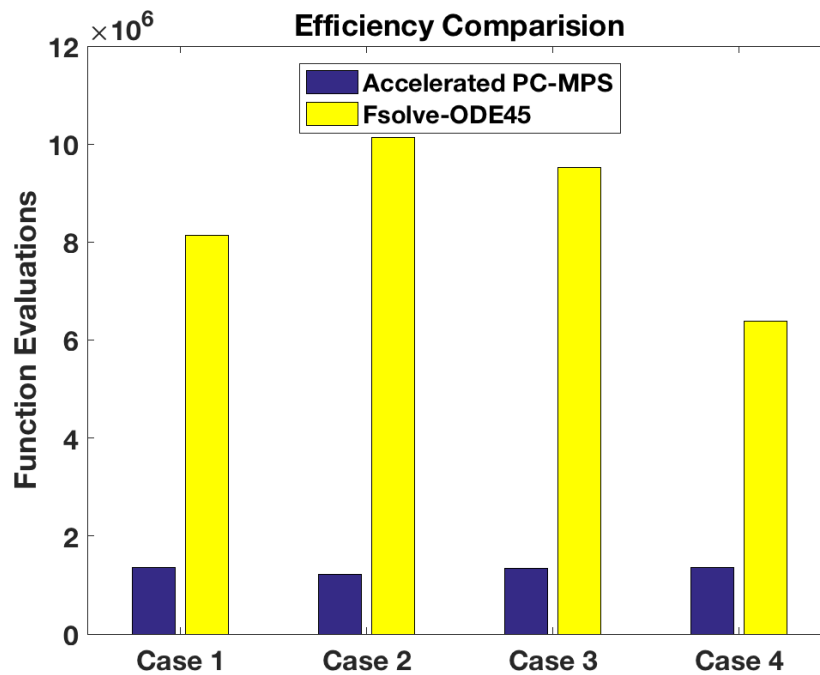


**Figure 9. Comparison of the number of high-fidelity spherical harmonic gravity force function evaluations.**

## ACKNOWLEDGMENT

Initial work was conducted by Woollands as a post-doctoral researcher at Texas A&M where she was funded by AFOSR (Staci Williams) and AFRL (Alok Das). Woollands continued and completed this work at the Jet Propulsion Laboratory, California Institute of Technology, under a contract with the National Aeronautics and Space Administration, and was funded by a Spontaneous Research and Technology Development Grant (Fred Hadaegh). Taheri and Junkins were funded by AFOSR (Staci Williams) and AFRL (Alok Das).

## REFERENCES

- [1] Longuski, J. M. and Williams, S. N., “Automated design of gravity-assist trajectories to Mars and the outer planets,” *Celestial Mechanics and Dynamical Astronomy*, Vol. 52, No. 3, 1991, pp. 207–220, doi:10.1007/BF00048484.
- [2] Izzo, D., Becerra, V. M., Myatt, D. R., Nasuto, S. J., and Bishop, J. M., “Search space pruning and global optimisation of multiple gravity assist spacecraft trajectories,” *Journal of Global Optimization*, Vol. 38, No. 2, 2007, pp. 283–296, doi:10.1007/s10898-006-9106-0.
- [3] Vasile, M. and Ceriotti, M., “8 Incremental Techniques for Global Space Trajectory Design,” *Spacecraft Trajectory Optimization*, edited by B. Conway, Vol. 29, 2010, pp. 202–237, doi:10.1017/CBO9780511778025.
- [4] Englander, J. A., Conway, B. A., and Williams, T., “Automated mission planning via evolutionary algorithms,” *Journal of Guidance, Control, and Dynamics*, Vol. 35, No. 6, 2012, pp. 1878–1887, doi:10.2514/1.54101.
- [5] Abdelkhalik, O. and Gad, A., “Dynamic-size multiple populations genetic algorithm for multigravity-assist trajectory optimization,” *Journal of Guidance, Control, and Dynamics*, Vol. 35, No. 2, 2012, pp. 520–529, doi:10.2514/1.54330.
- [6] Chilan, C. M. and Conway, B. A., “Automated design of multiphase space missions using hybrid optimal control,” *Journal of Guidance, Control, and Dynamics*, Vol. 36, No. 5, 2013, pp. 1410–1424.

- [7] Ellison, D. H., Conway, B. A., Englander, J. A., and Ozimek, M. T., "Analytic Gradient Computation for Bounded-Impulse Trajectory Models Using Two-Sided Shooting," *Journal of Guidance, Control, and Dynamics*, 2018, pp. 1–14.
- [8] Landau, D., "Efficient Maneuver Placement for Automated Trajectory Design," *Journal of Guidance, Control, and Dynamics*, Vol. 41, No. 7, 2018, pp. 1531–1541, doi:10.2514/1.G003172.
- [9] Betts, J. T., "Survey of numerical methods for trajectory optimization," *Journal of Guidance Control and Dynamics*, Vol. 21, No. 2, 1998, pp. 193–207, doi:10.2514/2.4231.
- [10] Shirazi, A., Ceberio, J., and Lozano, J. A., "Spacecraft trajectory optimization: A review of models, objectives, approaches and solutions," *Progress in Aerospace Sciences*, Vol. 102, 2018, pp. 76–98.
- [11] Bryson, A. E., *Applied optimal control: optimization, estimation and control*, CRC Press, 1975, chp.2.
- [12] Hargraves, C. R. and Paris, S. W., "Direct trajectory optimization using nonlinear programming and collocation," *Journal of Guidance, Control, and Dynamics*, Vol. 10, No. 4, 1987, pp. 338–342.
- [13] Herman, A. L. and Conway, B. A., "Direct optimization using collocation based on high-order Gauss-Lobatto quadrature rules," *Journal of Guidance, Control, and Dynamics*, Vol. 19, No. 3, 1996, pp. 592–599.
- [14] Betts, J., "Optimal interplanetary orbit transfers by direct transcription," *Journal of Astronautical Sciences*, Vol. 42, 1994, pp. 247–326.
- [15] Enright, P. and Conway, B., "Optimal finite-thrust spacecraft trajectories using collocation and nonlinear programming," *Journal of Guidance Dynamics and Control*, Vol. 14, 1991, pp. 981–985.
- [16] Enright, P. and Conway, B., "Discrete approximations to optimal trajectories using direct transcription and nonlinear programming," *Journal of Guidance Dynamics and Control*, Vol. 15, 1992, pp. 994–1002.
- [17] Seywald, H., "Trajectory optimization based on differential inclusion," *Journal of Guidance Dynamics and Control*, Vol. 17, 1994, pp. 480–487.
- [18] Miele, A. and Wang, T., "Optimal trajectories for Earth-to-Mars flight," *Journal of Optimal Control Theory Applied*, Vol. 95, 1997, pp. 467–499.
- [19] Miele, A. and Mancuso, S., "Optimal trajectories for Earth-Moon-Earth flight," *Acta Astron*, Vol. 49, 2001, pp. 59–71.
- [20] Miele, A. and Wang, T., "Multiple-subarc gradient-restoration algorithm, Part 1: Algorithm structure," *Journal of Optimal Control Theory Applied*, Vol. 116, 2003, pp. 1–17.
- [21] Miele, A. and Wang, T., "Multiple-subarc gradient-restoration algorithm, Part 2: Application to a multistage launch vehicle design," *Journal of Optimal Control Theory Applied*, Vol. 116, 2003, pp. 19–39.
- [22] Bruschi, R. and Vincent, T., "Numerical implementation of a second-order variational endpoint condition," *Journal of AIAA*, Vol. 8, 1970, pp. 2230–2235.
- [23] Hull, D., "Initial Lagrange multipliers for the shooting method," *Journal of Guidance Control and Dynamics*, Vol. 31, 2008, pp. 1490–1492.
- [24] Conway, B. and Mauro, P., "Optimal Low-Thrust Orbital Maneuvers via Indirect Swarming," *Journal of Optimal Theory Applied*, Vol. 162, 2014, pp. 272–292.
- [25] Taheri, E., Kolmanovskiy, I., and Atkins, E., "Enhanced smoothing technique for indirect optimization of minimum-fuel low-thrust trajectories," *Journal of Guidance, Control, and Dynamics*, Vol. 39, No. 11, 2016, pp. 2500–2511, doi:10.2514/1.G000379.
- [26] Junkins, J. L. and Taheri, E., "Exploration of Alternative State Vector Choices for Low Thrust Trajectory Optimization," *Journal of Guidance, Control, and Dynamics*, accepted for publication (doi: 10.2514/1.G003686).
- [27] Taheri, E. and Junkins, J., "A Generic Approach for Optimal Bang-Off-Bang Spacecraft Maneuvers," *41st Annual AAS Guidance & Control Conference, Breckenridge, Colorado*, 2018, AAS 18-088.
- [28] Taheri, E. and Junkins, J., "A Generic Approach for Optimal Bang-Off-Bang Spacecraft Maneuvers," *41st Annual AAS Guidance & Control Conference, Breckenridge, Colorado*, 2018, AAS 18-088.
- [29] Miele, A. and Iyer, R., "General Technique for Solving Nonlinear, Two-Point Boundary value Problems Via the Method of Particular Solutions," *Journal of Optimization Theory and Applications*, Vol. 5, No. 5, 1970, pp. 392–399.
- [30] Kelso, T. et al., "Analysis of the Iridium 33-Cosmos 2251 collision," *Advances in the Astronautical Sciences*, Vol. 135, No. 2, 2009, pp. 1099–1112.
- [31] Pardini, C. and Anselmo, L., "Assessment of the consequences of the Fengyun-1C breakup in low Earth orbit," *Advances in Space Research*, Vol. 44, No. 5, 2009, pp. 545–557.
- [32] Jones, K., Fuentes, K., and Wright, D., "A Minefield in Earth Orbit: How Space Debris is Spinning Out of Control," *Scientific American*, 2012.
- [33] Lawden, D. F., *Optimal trajectories for space navigation*, Butterworths, 1963, chp.3.

- [34] Coles, W. and Sherman, T., "Convergence of successive approximations for nonlinear two-point boundary value problems," *SIAM Journal on Applied Mathematics*, Vol. 15, No. 2, 1967, pp. 426–433.
- [35] Van de Craats, J., "On the region of convergence of Picard's iteration," *ZAMM-Journal of Applied Mathematics and Mechanics/Zeitschrift für Angewandte Mathematik und Mechanik*, Vol. 52, No. 8, 1972, pp. 487–491.
- [36] Read, J., Bani Younes, A., and Junkins, J., "Efficient Orbit Propagation of Orbital Elements Using Modified Chebyshev-Picard Iteration Method," *Computational Modelling in Engineering & Sciences*, Vol. 111, 2016, pp. 65–82.
- [37] Clenshaw, C. W. and Norton, H. J., "The Solution of Nonlinear Ordinary Differential Equations in Chebyshev Series," *The Computer Journal*, Vol. 6, 1963, pp. 88–92.
- [38] Feagin, T., "The Numerical Solution of Two-Point Boundary Value Problems using Chebyshev Polynomial Series," *PhD. Dissertation, University of Texas, Austin, Texas, USA*, 1972.
- [39] Feagin, T. and Nacozy, P., "Matrix Formulation of the Picard Method for Parallel Computation," *Celestial Mechanics and Dynamical Astronomy*, Vol. 29, 1983, pp. 107–115.
- [40] Shaver, J., "Formulation and Evaluation of Parallel Algorithms for the Orbit Determination Problem," *Ph.D. Dissertation, Department of Aeronautics and Astronautics, MIT, Cambridge, MA*, 1980.
- [41] Fukushima, T., "Vector Integration of Dynamical Motions by the Picard-Chebyshev Method," *The Astronomical Journal*, Vol. 113, 1997, pp. 2325–2328.
- [42] Bai, X. and Junkins, J., "Modified Chebyshev-Picard Iteration Methods for Solution of Initial Value Problems," *Advances in the Astronautical Sciences*, Vol. 139, 2011, pp. 345–362.
- [43] Bai, X. and Junkins, J., "Modified Chebyshev-Picard Iteration Methods for Solution of Boundary Value Problems," *Advances in the Astronautical Sciences*, Vol. 140, 2011, pp. 381–400.
- [44] Bai, X., "Modified Chebyshev-Picard Iteration for Solution of Initial Value and Boundary Value Problems," *PhD. Dissertation, Texas A&M, College Station, Texas, USA*, 2010.
- [45] Junkins, J., Bani Younes, A., Woollands, R., and Bai, X., "Orthogonal Approximation in Higher Dimensions: Applications in Astrodynamics," *AAS 12-634, JN Juang Astrodynamics Symp*, 2012.
- [46] Junkins, J., Bani Younes, A., Woollands, R., and Bai, X., "Picard Iteration, Chebyshev Polynomial and Chebyshev Picard Methods: Application in Astrodynamics," *Journal of the Astronautical Sciences*, 2013.
- [47] Junkins, J., Bani Younes, A., Woollands, R., and Bai, X., "Efficient and Adaptive Orthogonal Finite Element Representation of the Geopotential," *Journal of the Astronautical Sciences*, accepted 2016.
- [48] Bani Younes, A., "Orthogonal Polynomial Approximation in Higher Dimensions: Applications in Astrodynamics," *PhD. Dissertation, Texas A&M, College Station, Texas, USA*, 2013.
- [49] Macomber, B., "Enhancements of Chebyshev-Picard Iteration Efficiency for Generally Perturbed Orbits and Constrained Dynamics Systems," *PhD. Dissertation, Texas A&M University, College Station, Texas, USA*, 2015.
- [50] Macomber, B., Probe, A., Woollands, R., Read, J., and Junkins, J., "Enhancements of Modified Chebyshev-Picard Iteration Efficiency for Perturbed Orbit Propagation," *Computational Modelling in Engineering & Sciences*, Vol. 111, 2016, pp. 29–64.
- [51] Junkins, J. and Woollands, R., "Nonlinear Differential Equation Solvers via Adaptive Picard-Chebyshev Iteration: Applications in Astrodynamics," *AAS/AIAA Astrodynamics Specialist Conference*, 2017.
- [52] Woollands, R. and Junkins, J., "Nonlinear Differential Equation Solvers via Adaptive Picard-Chebyshev Iteration: Applications in Astrodynamics," *Journal of Guidance, Control and Dynamics*, accepted, December 2018.
- [53] Woollands, R., Read, J., Probe, A., and Junkins, J., "Multiple Revolution Solutions for the Perturbed Lambert Problem using the Method of Particular Solutions and Picard Iteration," *Journal of Astronautical Sciences*, accepted 2017.
- [54] Kéchichian, J. A., "Inclusion of higher order harmonics in the modeling of optimal low-thrust orbit transfer," *The Journal of the Astronautical Sciences*, Vol. 56, No. 1, 2008, pp. 41–70.
- [55] Kechichian, J. A., "The treatment of the earth oblateness effect in trajectory optimization in equinoctial coordinates," *Acta astronautica*, Vol. 40, No. 1, 1997, pp. 69–82.
- [56] Taheri, E. and Junkins, L. J., "How many impulses redux," *The Journal of the Astronautical Sciences*, 2018, under review.
- [57] Handelsman, M. and Lion, P., "Primer vector on fixed-time impulsive trajectories." *AIAA Journal*, Vol. 6, No. 1, 1968, pp. 127–132.
- [58] Graham, K. F. and Rao, A. V., "Minimum-time trajectory optimization of multiple revolution low-thrust earth-orbit transfers," *Journal of Spacecraft and Rockets*, Vol. 52, No. 3, 2015, pp. 711–727.